Phase reduction approach to elastohydrodynamic synchronization of beating flagella

Yoji Kawamura[1,2,*] and Remi Tsubaki[2]

[1]*Department of Mathematical Science and Advanced Technology, Japan Agency for Marine-Earth Science and Technology, Yokohama 236-0001, Japan*

[2]*Research and Development Center for Marine Biosciences, Japan Agency for Marine-Earth Science and Technology, Yokosuka 237-0061, Japan*

(Received 12 July 2017; published 12 February 2018)

We formulate a theory for the phase reduction of a beating flagellum. The theory enables us to describe the dynamics of a beating flagellum in a systematic manner using a single variable called the phase. The theory can also be considered as a phase reduction method for the limit-cycle solutions in infinite-dimensional dynamical systems, namely, the limit-cycle solutions to partial differential equations representing beating flagella. We derive the phase sensitivity function, which quantifies the phase response of a beating flagellum to weak perturbations applied at each point and at each time. Using the phase sensitivity function, we analyze the phase synchronization between a pair of beating flagella through hydrodynamic interactions at a low Reynolds number.

DOI: 10.1103/PhysRevE.97.022212

I. INTRODUCTION

A population of coupled limit-cycle oscillators exhibits a rich variety of synchronization phenomena [1–3]. Each oscillator is typically described by a limit-cycle solution to an ordinary differential equation. A phase reduction method [1–10], which enables us to describe the dynamics of an oscillator using a single degree of freedom called the phase, has been successfully applied to analyze the synchronization properties of weakly coupled oscillators. Consequently, collective synchronization exhibited by coupled phase oscillators has been well investigated for globally coupled systems, nonlocally coupled systems, and complex network systems [1–6,9–15].

Recently, hydrodynamic synchronization, which indicates the synchronization of oscillators via hydrodynamic interactions, has attracted considerable attention [16–21]. For example, this synchronization phenomenon has been intensively investigated through experiments such as *Chlamydomonas* and *Volvox* [22–27], wherein their beating flagella can be considered as limit-cycle oscillators. In particular, both the experimental and theoretical studies [27,28] have clearly demonstrated that a pair of adjacent beating flagella can be in-phase synchronized only through hydrodynamic interactions at a low Reynolds number. Further, the theoretical study [28] described a beating flagellum using a limit-cycle solution to a partial differential equation.

Moreover, we recently formulated a theory for the phase reduction of limit-cycle solutions to the following partial differential equations: nonlinear Fokker-Planck equations representing collective oscillations of globally coupled noisy dynamical elements [29,30], fluid equations representing oscillatory thermal convection in Hele-Shaw cells [31–33], and reaction-diffusion equations representing rhythmic spatiotemporal patterns in chemical and biological systems [34,35]. The theory can be considered as a generalization of the conventional phase reduction method for limit-cycle solutions to ordinary differential equations.

In this paper, we formulate a theory for the phase reduction of a beating flagellum represented by a partial differential equation proposed by Goldstein *et al.* in Ref. [28]. The theory can also be considered as a phase reduction method for limit-cycle solutions to partial differential equations. We derive the phase sensitivity function, which quantifies the phase response of a beating flagellum to weak perturbations applied at each point and at each time, and subsequently analyze the mutual synchronization between a pair of beating flagella through hydrodynamic interactions at a low Reynolds number.

This paper is organized as follows. In Sec. II, we formulate a theory for the phase description of beating flagella. In Sec. III with Appendixes A and B, we perform a numerical analysis of beating flagella. Concluding remarks are given in Sec. IV.

II. PHASE DESCRIPTION OF BEATING FLAGELLA

In this section, we formulate a theory for the phase description of beating flagella represented by fourth-order nonlinear partial differential equations. The formulation procedure is similar to that performed in Refs. [29–33].

A. Dimensionless form of model equations

We consider the following phenomenological model proposed by Goldstein *et al.* in Ref. [28] for a beating flagellum:

$$\frac{\partial}{\partial t}h(x,t) = \mathcal{N}(h). \tag{1}$$

The variable $h(x,t)$ denotes the vertical displacement at the point x and time t. The right-hand side of Eq. (1) is given by [36]

$$\mathcal{N}(h) = -c\frac{\partial h}{\partial x} - 2\frac{\partial^2 h}{\partial x^2} - \frac{\partial^4 h}{\partial x^4} + \left(\frac{\partial^2 h}{\partial x^2}\right)^3. \tag{2}$$

*ykawamura@jamstec.go.jp

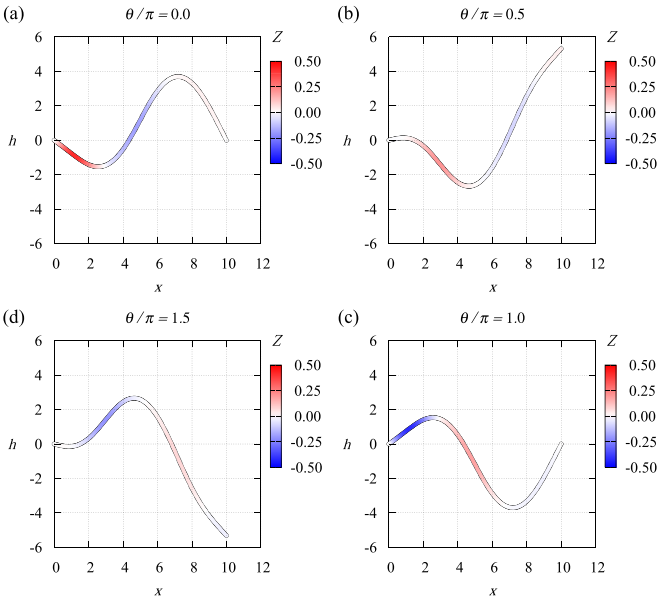

FIG. 1. Snapshots of both the limit-cycle solution $h_0(x,\theta)$ and phase sensitivity function $Z(x,\theta)$ for (a) $\theta/\pi = 0.0$, (b) $\theta/\pi = 0.5$, (c) $\theta/\pi = 1.0$, and (d) $\theta/\pi = 1.5$. The parameters are $c = 1$ and $L = 10$. The frequency is $\omega \simeq 0.67$.

Note that Eq. (2) possesses the following property: $\mathcal{N}(-h) = -\mathcal{N}(h)$. The flagellum is assumed to be hinged at the left end and free at the right end. In other words, the boundary condition at the left end ($x = 0$) is given by

$$h(x,t)\Big|_{x=0} = \frac{\partial^2 h(x,t)}{\partial x^2}\Big|_{x=0} = 0 \tag{3}$$

and the boundary condition at the right end ($x = L$) is given by

$$\frac{\partial^2 h(x,t)}{\partial x^2}\Big|_{x=L} = \frac{\partial^3 h(x,t)}{\partial x^3}\Big|_{x=L} = 0. \tag{4}$$

In this model, the left-right symmetry, i.e., the reflection symmetry with respect to x, does not exist, but the up-down symmetry, i.e., the reflection symmetry with respect to h, exists. In other words, the variable $-h(x,t)$ satisfies exactly the same equation for the variable $h(x,t)$.

B. Limit-cycle solution and its Floquet-type system

In general, a stable limit-cycle solution to Eq. (1) can be described by [e.g., see Figs. 1 and 2(a) in Sec. III]

$$h(x,t) = h_0(x,\theta(t)), \quad \dot{\theta}(t) = \omega. \tag{5}$$

The phase and frequency are denoted by θ and ω, respectively. The limit-cycle solution $h_0(x,\theta)$ possesses the following 2π periodicity in θ: $h_0(x,\theta + 2\pi) = h_0(x,\theta)$. Substituting Eq. (5) into Eq. (1), we determine that the limit-cycle solution $h_0(x,\theta)$ satisfies

$$\omega\frac{\partial}{\partial\theta}h_0(x,\theta) = \mathcal{N}(h_0). \tag{6}$$

Let $u(x,\theta,t)$ represent a small disturbance added to the limit-cycle solution $h_0(x,\theta)$, and consider a slightly perturbed solution

$$h(x,t) = h_0(x,\theta(t)) + u(x,\theta(t),t). \tag{7}$$

Equation (1) is subsequently linearized with respect to $u(x,\theta,t)$ as

$$\frac{\partial}{\partial t}u(x,\theta,t) = \mathcal{L}(x,\theta)u(x,\theta,t). \tag{8}$$

Further, the linear operator $\mathcal{L}(x,\theta)$ is explicitly given by

$$\mathcal{L}(x,\theta)u(x,\theta) = \left[\mathcal{J}(x,\theta) - \omega\frac{\partial}{\partial\theta}\right]u(x,\theta), \tag{9}$$

where

$$\mathcal{J}(x,\theta)u(x,\theta) = -c\frac{\partial u}{\partial x} - 2\frac{\partial^2 u}{\partial x^2} - \frac{\partial^4 u}{\partial x^4} + 3\left(\frac{\partial^2 h_0}{\partial x^2}\right)^2\frac{\partial^2 u}{\partial x^2}. \tag{10}$$

In Eq. (9), we omitted the t dependence of the function $u(x,\theta,t)$ and denoted it as $u(x,\theta)$ because we consider only the eigenvalue problem of the linear operator $\mathcal{L}(x,\theta)$ and thus the t dependence of the function u does not appear hereafter. Note that the linear operator $\mathcal{L}(x,\theta)$ is periodic with respect to θ. Therefore, Eq. (8) is a Floquet-type system with a periodic linear operator $\mathcal{L}(x,\theta)$, which has the zero eigenvalue associated with the spontaneous breaking of temporal translational symmetry.

C. Adjoint operator and adjoint boundary conditions

Defining the inner product of the two functions as

$$[\![u^*(x,\theta), u(x,\theta)]\!] = \frac{1}{2\pi}\int_0^{2\pi} d\theta \int_0^L dx\, u^*(x,\theta)u(x,\theta), \tag{11}$$

we introduce the adjoint operator of the linear operator $\mathcal{L}(x,\theta)$ by

$$[\![u^*(x,\theta), \mathcal{L}(x,\theta)u(x,\theta)]\!] = [\![\mathcal{L}^*(x,\theta)u^*(x,\theta), u(x,\theta)]\!] + \mathcal{S}[u^*(x,\theta), u(x,\theta)]. \tag{12}$$

By partial integration, the adjoint operator $\mathcal{L}^*(x,\theta)$ is explicitly obtained as

$$\mathcal{L}^*(x,\theta)u^*(x,\theta) = \left[\mathcal{J}^*(x,\theta) + \omega\frac{\partial}{\partial\theta}\right]u^*(x,\theta), \tag{13}$$

where

$$\mathcal{J}^*(x,\theta)u^*(x,\theta) = c\frac{\partial u^*}{\partial x} - 2\frac{\partial^2 u^*}{\partial x^2} - \frac{\partial^4 u^*}{\partial x^4} + 3\frac{\partial^2}{\partial x^2}\left\{u^*\left(\frac{\partial^2 h_0}{\partial x^2}\right)^2\right\}. \tag{14}$$

The bilinear concomitant $\mathcal{S}[u^*(x,\theta), u(x,\theta)]$ is given by (see also, e.g., Refs. [37,38] for mathematical terms)

$$\mathcal{S}[u^*(x,\theta), u(x,\theta)] = \frac{1}{2\pi}\int_0^{2\pi} d\theta\left[-cu^*u - 2u^*\frac{\partial u}{\partial x} + 2\frac{\partial u^*}{\partial x}u - u^*\frac{\partial^3 u}{\partial x^3}\right.$$

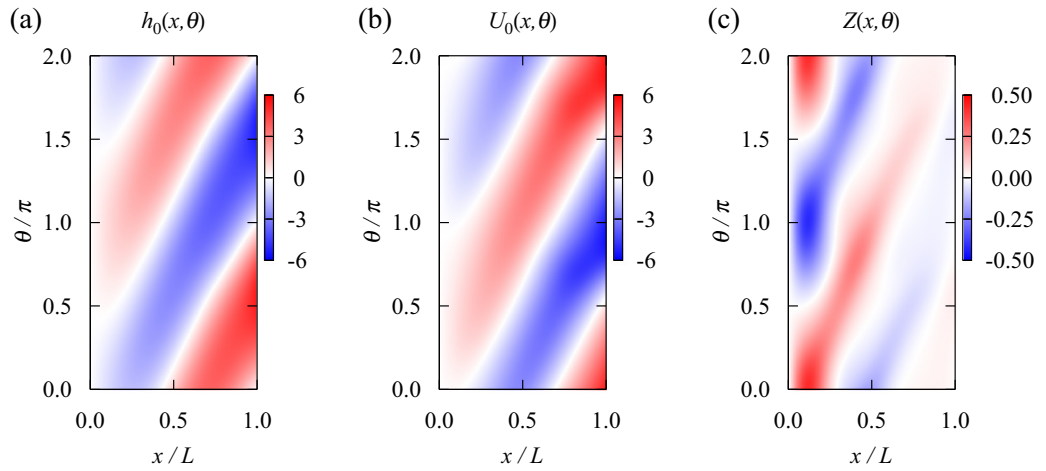

FIG. 2. (a) Limit-cycle solution $h_0(x,\theta)$. (b) Floquet zero eigenfunction $U_0(x,\theta) = \partial h_0(x,\theta)/\partial\theta$. (c) Phase sensitivity function $Z(x,\theta) = U_0^*(x,\theta)$.

$$+\frac{\partial u^*}{\partial x}\frac{\partial^2 u}{\partial x^2} - \frac{\partial^2 u^*}{\partial x^2}\frac{\partial u}{\partial x} + \frac{\partial^3 u^*}{\partial x^3}u\Bigg]_{x=0}^{x=L}$$
$$+\frac{1}{2\pi}\int_0^{2\pi} d\theta\left[3u^*\left(\frac{\partial^2 h_0}{\partial x^2}\right)^2\frac{\partial u}{\partial x}\right.$$
$$\left.-3\frac{\partial}{\partial x}\left\{u^*\left(\frac{\partial^2 h_0}{\partial x^2}\right)^2\right\}u\right]_{x=0}^{x=L}$$
$$+\frac{1}{2\pi}\int_0^L dx\,[-\omega u^* u]_{\theta=0}^{\theta=2\pi}. \tag{15}$$

The second term on the right-hand side of Eq. (15) is zero owing to the following boundary conditions for the limit-cycle solution $h_0(x,\theta)$:

$$\left.\frac{\partial^2 h_0(x,\theta)}{\partial x^2}\right|_{x=0} = \left.\frac{\partial^2 h_0(x,\theta)}{\partial x^2}\right|_{x=L} = 0. \tag{16}$$

The third term is zero owing to the 2π periodicity of both $u(x,\theta)$ and $u^*(x,\theta)$ in θ as

$$u(x,\theta)|_{\theta=0} = u(x,\theta)|_{\theta=2\pi}, \tag{17}$$

$$u^*(x,\theta)|_{\theta=0} = u^*(x,\theta)|_{\theta=2\pi}. \tag{18}$$

As in the limit-cycle solution $h_0(x,\theta)$, the boundary condition at the left end ($x = 0$) for $u(x,\theta)$ is given by

$$\left.u(x,\theta)\right|_{x=0} = \left.\frac{\partial^2 u(x,\theta)}{\partial x^2}\right|_{x=0} = 0 \tag{19}$$

and the boundary condition at the right end ($x = L$) for $u(x,\theta)$ is given by

$$\left.\frac{\partial^2 u(x,\theta)}{\partial x^2}\right|_{x=L} = \left.\frac{\partial^3 u(x,\theta)}{\partial x^3}\right|_{x=L} = 0. \tag{20}$$

Since the first term on the right-hand side of Eq. (15) is zero, the adjoint boundary condition at the left end ($x = 0$) is given by

$$\left.u^*(x,\theta)\right|_{x=0} = \left.\frac{\partial^2 u^*(x,\theta)}{\partial x^2}\right|_{x=0} = 0 \tag{21}$$

and the adjoint boundary condition at the right end ($x = L$) is given by

$$\left(2+\frac{\partial^2}{\partial x^2}\right)u^*(x,\theta)\Big|_{x=L}$$
$$= \left(-c + 2\frac{\partial}{\partial x} + \frac{\partial^3}{\partial x^3}\right)u^*(x,\theta)\Big|_{x=L} = 0. \tag{22}$$

Under these conditions, the bilinear concomitant is zero, $\mathcal{S}[u^*(x,\theta), u(x,\theta)] = 0$.

D. Floquet zero eigenfunctions and their normalization

In the calculation below, we use the Floquet eigenfunctions associated with the zero eigenvalue of $\mathcal{L}(x,\theta)$ and $\mathcal{L}^*(x,\theta)$; these eigenfunctions satisfy [e.g., see Figs. 2(b) and 2(c) in Sec. III]

$$\mathcal{L}(x,\theta)U_0(x,\theta) = \left[\mathcal{J}(x,\theta) - \omega\frac{\partial}{\partial\theta}\right]U_0(x,\theta) = 0, \tag{23}$$

$$\mathcal{L}^*(x,\theta)U_0^*(x,\theta) = \left[\mathcal{J}^*(x,\theta) + \omega\frac{\partial}{\partial\theta}\right]U_0^*(x,\theta) = 0. \tag{24}$$

The Floquet zero eigenfunction $U_0(x,\theta)$ can be chosen as

$$U_0(x,\theta) = \frac{\partial}{\partial\theta}h_0(x,\theta), \tag{25}$$

which is confirmed by differentiating Eq. (5) with respect to θ. From Eqs. (6) and (25), the Floquet zero eigenfunction $U_0(x,\theta)$ satisfies

$$\omega U_0(x,\theta) = \mathcal{N}(h_0). \tag{26}$$

Using the inner product with the Floquet zero eigenfunction $U_0(x,\theta)$, the adjoint zero eigenfunction $U_0^*(x,\theta)$ is normalized as

$$[\![U_0^*(x,\theta), U_0(x,\theta)]\!]$$
$$= \frac{1}{2\pi}\int_0^{2\pi} d\theta\int_0^L dx\, U_0^*(x,\theta)U_0(x,\theta) = 1. \tag{27}$$

Note that the following equation holds (see also Refs. [4,29–33]):

$$\begin{aligned}&\frac{\partial}{\partial\theta}\left[\int_0^L dx\, U_0^*(x,\theta)U_0(x,\theta)\right]\\&=\int_0^L dx\left[U_0^*(x,\theta)\frac{\partial}{\partial\theta}U_0(x,\theta)+U_0(x,\theta)\frac{\partial}{\partial\theta}U_0^*(x,\theta)\right]\\&=\frac{1}{\omega}\int_0^L dx\,[U_0^*(x,\theta)\mathcal{J}(x,\theta)U_0(x,\theta)\\&\quad-U_0(x,\theta)\mathcal{J}^*(x,\theta)U_0^*(x,\theta)]=0.\end{aligned}\tag{28}$$

Therefore, the following normalization condition is independently satisfied for each θ:

$$\int_0^L dx\, U_0^*(x,\theta)U_0(x,\theta)=1.\tag{29}$$

Further, we note a numerical method for obtaining the adjoint zero eigenfunction $U_0^*(x,\theta)$. From Eq. (24), the adjoint zero eigenfunction satisfies

$$\omega\frac{\partial}{\partial\theta}U_0^*(x,\theta)=-\mathcal{J}^*(x,\theta)U_0^*(x,\theta),\tag{30}$$

which can be transformed into

$$\frac{\partial}{\partial s}U_0^*(x,-\omega s)=\mathcal{J}^*(x,-\omega s)U_0^*(x,-\omega s)\tag{31}$$

by substituting $\theta=-\omega s$. A relaxation method using Eq. (31), which can also be called the adjoint method (see Refs. [4–10] for ordinary differential equations and Refs. [29–34] for partial differential equations), is convenient to obtain the adjoint zero eigenfunction. In the following two subsections, we derive the phase equations of beating flagella using the limit-cycle solution $h_0(x,\theta)$, Floquet zero eigenfunction $U_0(x,\theta)$, and adjoint zero eigenfunction $U_0^*(x,\theta)$.

E. Beating flagella with weak perturbations

In this subsection, we consider a beating flagellum with a weak perturbation described by the following equation:

$$\frac{\partial}{\partial t}h(x,t)=\mathcal{N}(h)+\epsilon p(x,t).\tag{32}$$

The weak perturbation is denoted by $\epsilon p(x,y,t)$. Here, we assume that the perturbed solution is always near the orbit of the limit-cycle solution $h_0(x,\theta)$. Further, using the adjoint zero eigenfunction $U_0^*(x,\theta)$, we project the dynamics of the perturbed equation (32) onto the unperturbed solution $h_0(x,\theta)$ as

$$\begin{aligned}\dot\theta(t)&=\int_0^L dx\, U_0^*(x,\theta)[\mathcal{N}(h)+\epsilon p(x,t)]\\&\simeq\int_0^L dx\, U_0^*(x,\theta)[\mathcal{N}(h_0)+\epsilon p(x,t)]\\&=\int_0^L dx\, U_0^*(x,\theta)[\omega U_0(x,\theta)+\epsilon p(x,t)]\\&=\omega+\epsilon\int_0^L dx\, U_0^*(x,\theta)p(x,t),\end{aligned}\tag{33}$$

where we approximated $h(x,t)$ by the unperturbed solution $h_0(x,\theta)$ and used Eqs. (26) and (29). Therefore, the phase equation describing the beating flagellum with weak perturbation is approximately obtained in the following form:

$$\dot\theta(t)=\omega+\epsilon\int_0^L dx\, Z(x,\theta)p(x,t),\tag{34}$$

where the *phase sensitivity function* is defined as [e.g., see Figs. 1 and 2(c) in Sec. III]

$$Z(x,\theta)=U_0^*(x,\theta).\tag{35}$$

The phase equation (34) is the main result of this paper. The phase sensitivity function $Z(x,\theta)$ quantifies the phase response of the beating flagellum to weak perturbations applied at each point and at each time.

When the perturbation is given by $p(x,t)=q(t)$, Eq. (34) can also be written in the following form:

$$\dot\theta(t)=\omega+\epsilon\zeta(\theta)q(t),\tag{36}$$

where the *effective phase sensitivity function* is given by [e.g., see Fig. 3(b) in Sec. III]

$$\zeta(\theta)=\int_0^L dx\, Z(x,\theta).\tag{37}$$

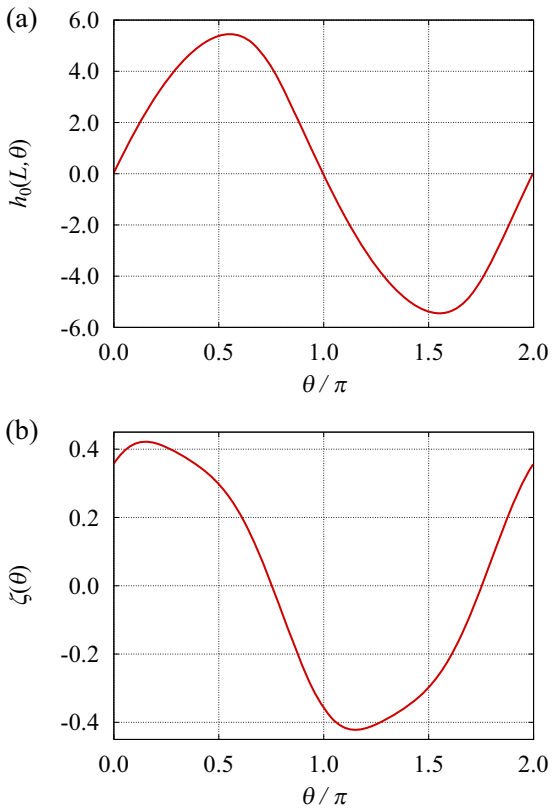

FIG. 3. (a) Periodic motion of the flagellar tip, $h_0(L,\theta)$. (b) Effective phase sensitivity function $\zeta(\theta)$.

F. Hydrodynamically coupled beating flagella

In this subsection, we consider a pair of hydrodynamically coupled beating flagella described by the following

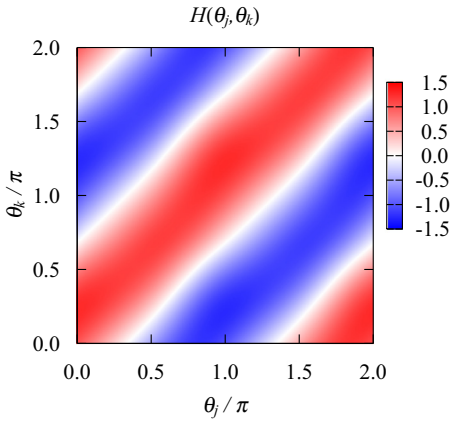

FIG. 4. Hydrodynamic interaction function $H(\theta_j,\theta_k)$.

equation [28]:

$$\frac{\partial}{\partial t}h_j(x,t) = \mathcal{N}(h_j) + \epsilon\,\mathcal{N}(h_k), \tag{38}$$

for $(j,k) = (1,2)$ or $(2,1)$. The second term on the right-hand side of Eq. (38) represents hydrodynamic interactions. The effective coupling intensity is denoted by ϵ, which is a small parameter [39]. Here, we assume that the waveforms of two flagella are only slightly perturbed and persist even when hydrodynamic interactions between the two flagella exist. As in Sec. II E, using the adjoint zero eigenfunction $U_0^*(x,\theta_j)$, we project the dynamics of the equation (38) onto the unperturbed solution as

$$\begin{aligned}\dot{\theta}_j(t) &= \int_0^L dx\, U_0^*(x,\theta_j)[\mathcal{N}(h_j) + \epsilon\,\mathcal{N}(h_k)] \\ &\simeq \int_0^L dx\, U_0^*(x,\theta_j)[\mathcal{N}(h_0(x,\theta_j)) + \epsilon\,\mathcal{N}(h_0(x,\theta_k))] \\ &= \int_0^L dx\, U_0^*(x,\theta_j)[\omega U_0(x,\theta_j) + \epsilon\omega U_0(x,\theta_k)] \\ &= \omega + \epsilon\omega\int_0^L dx\, U_0^*(x,\theta_j)U_0(x,\theta_k),\end{aligned} \tag{39}$$

where we approximated $h_j(x,t)$ by the unperturbed solution $h_0(x,\theta_j)$ and used Eqs. (26) and (29). Therefore, the phase equation describing a pair of hydrodynamically coupled beating flagella is approximately obtained in the following form:

$$\dot{\theta}_j(t) = \omega + \epsilon\omega H(\theta_j,\theta_k), \tag{40}$$

where the *hydrodynamic interaction function* is given by (e.g., see Fig. 4 in Sec. III)

$$H(\theta_j,\theta_k) = \int_0^L dx\, U_0^*(x,\theta_j)U_0(x,\theta_k). \tag{41}$$

From Eq. (29), the hydrodynamic interaction function takes the value of unity for $\theta_j = \theta_k = \theta$, i.e.,

$$H(\theta,\theta) = \int_0^L dx\, U_0^*(x,\theta)U_0(x,\theta) = 1. \tag{42}$$

The hydrodynamic interaction function $H(\theta_j,\theta_k)$ given by Eq. (41) depends on the phases of both beating flagella.

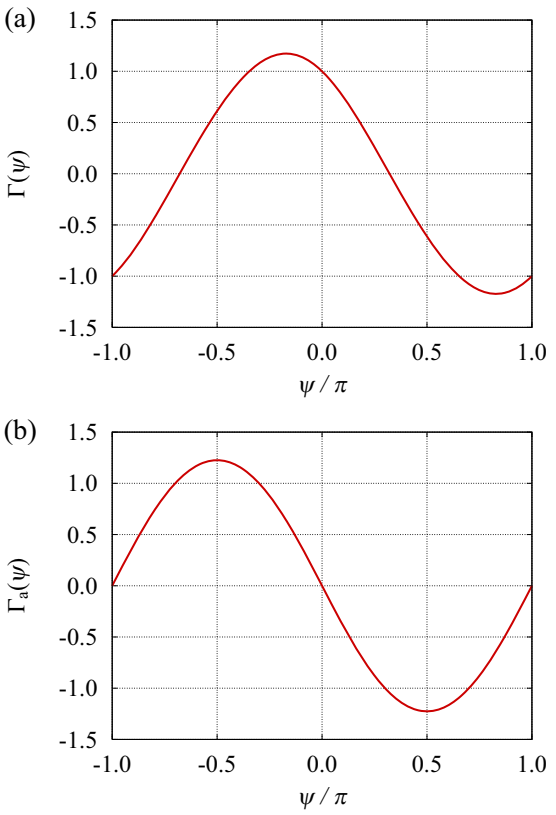

FIG. 5. (a) Phase coupling function $\Gamma(\psi)$. (b) Antisymmetric component of the phase coupling function, $\Gamma_a(\psi)$.

By applying the averaging method [2], Eq. (40) can be written in the following form:

$$\dot{\theta}_j(t) = \omega + \epsilon\omega\Gamma(\theta_j - \theta_k), \tag{43}$$

where the *phase coupling function* is given by [e.g., see Fig. 5(a) in Sec. III]

$$\Gamma(\theta_j - \theta_k) = \frac{1}{2\pi}\int_0^{2\pi} d\lambda\, H(\lambda + \theta_j, \lambda + \theta_k). \tag{44}$$

The phase coupling function $\Gamma(\theta_j - \theta_k)$ depends only on the phase difference, $\theta_j - \theta_k$.

Let the phase difference be defined as $\psi(t) = \theta_1(t) - \theta_2(t)$. From Eq. (43), we obtain the following equation by subtraction:

$$\dot{\psi}(t) = \epsilon\omega\Gamma_a(\psi), \tag{45}$$

where the antisymmetric component of the phase coupling function is defined as [e.g., see Fig. 5(b) in Sec. III]

$$\Gamma_a(\psi) = \Gamma(\psi) - \Gamma(-\psi). \tag{46}$$

By definition, $\Gamma_a(-\psi) = -\Gamma_a(\psi)$ holds. From Eqs. (41) and (44), the phase coupling function $\Gamma(\psi)$ can also be written in the following form:

$$\Gamma(\psi) = \frac{1}{2\pi}\int_0^{2\pi} d\lambda \int_0^L dx\, U_0^*(x,\lambda + \psi)U_0(x,\lambda). \tag{47}$$

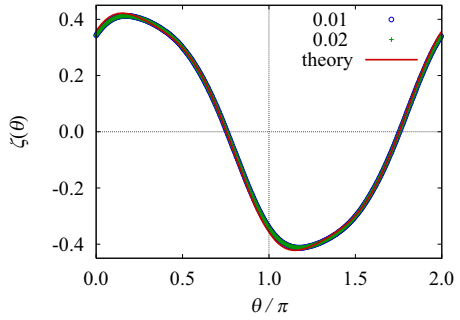

FIG. 6. Comparison of the effective phase sensitivity function $\zeta(\theta)$ between the two direct numerical simulations ($\epsilon = 0.01, 0.02$) and the theoretical curve (theory).

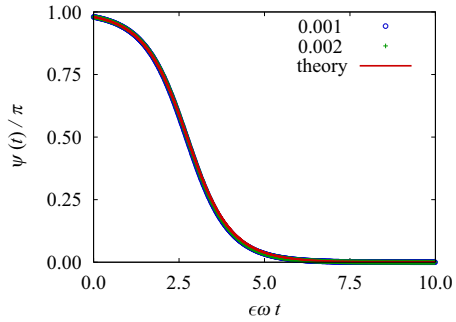

FIG. 7. Comparison of the time evolution of the phase difference, $\psi(t)/\pi$ vs $\epsilon\omega t$, between the two direct numerical simulations ($\epsilon = 0.001, 0.002$) and the theoretical curve (theory).

From Eq. (29), the phase coupling function satisfies

$$\Gamma(0) = \frac{1}{2\pi}\int_0^{2\pi} d\lambda \int_0^L dx\, U_0^*(x,\lambda)U_0(x,\lambda) = 1. \quad (48)$$

In summary, a pair of hydrodynamically coupled beating flagella represented by a set of partial differential equations (38) can be reduced to a single ordinary differential equation (45). Note that the theory can be extended to include effects of frequency mismatch and/or noise.

Finally, from Eqs. (40) and (42), for the in-phase synchronized state ($\theta_j = \theta_k = \theta$), the phase equation can be written in the following form: $\dot{\theta}(t) = (1+\epsilon)\omega$, which is also derived from Eqs. (43) and (48). Further, for the in-phase synchronized state ($h_j = h_k = h$), Eq. (38) can be written in the following form: $\partial_t h(x,t) = (1+\epsilon)\mathcal{N}(h)$, which also gives the frequency as $(1+\epsilon)\omega$. Under the situation considered in this subsection, the hydrodynamic interaction leads to the positive frequency shift for the in-phase synchronized state.

III. NUMERICAL ANALYSIS OF BEATING FLAGELLA

In this section, we perform a numerical analysis of beating flagella to illustrate the theory formulated in Sec. II. The numerical methods for model equations and adjoint equations are summarized in Appendixes A and B, respectively. The parameters are fixed at $c = 1$ and $L = 10$. The number of grid points is $N+1 = 201$ for the theoretical values shown in Figs. 1–7, whereas it is $N+1 = 101$ for the simulation results with a small parameter ϵ shown in Figs. 6 and 7.

A. Phase sensitivity functions

Figure 1 shows the snapshots of both the limit-cycle solution $h_0(x,\theta)$ and phase sensitivity function $Z(x,\theta)$ for $\theta/\pi = 0.0$, 0.5, 1.0, and 1.5. The limit-cycle solution $h_0(x,\theta)$ is represented by points (x,h), and the phase sensitivity function $Z(x,\theta)$ is shown in colors. The frequency is $\omega \simeq 0.67$.

Figure 2 shows the limit-cycle solution $h_0(x,\theta)$, Floquet zero eigenfunction $U_0(x,\theta) = \partial h_0(x,\theta)/\partial\theta$, and phase sensitivity function $Z(x,\theta) = U_0^*(x,\theta)$. Owing to the up-down symmetry mentioned in Sec. II A, these functions satisfy

$$h_0(x,\theta+\pi) = -h_0(x,\theta), \quad (49)$$

$$U_0(x,\theta+\pi) = -U_0(x,\theta), \quad (50)$$

$$U_0^*(x,\theta+\pi) = -U_0^*(x,\theta). \quad (51)$$

As shown in Fig. 2(c), the absolute values of the phase sensitivity function $Z(x,\theta)$ in the left region ($x < L/2$) are larger than those in the right region ($x > L/2$).

Figure 3(a) shows the periodic motion of the flagellar tip, $h_0(L,\theta)$. As in Eq. (49), the periodic motion of the flagellar tip possesses the following symmetry: $h_0(L,\theta+\pi) = -h_0(L,\theta)$.

Figure 3(b) shows the effective phase sensitivity function, $\zeta(\theta) = \int_0^L dx\, Z(x,\theta)$, given by Eq. (37). Owing to Eq. (51), the effective phase sensitivity function satisfies

$$\zeta(\theta+\pi) = -\zeta(\theta). \quad (52)$$

B. Phase coupling functions

Figure 4 shows the hydrodynamic interaction function $H(\theta_j,\theta_k)$ given by Eq. (41). As shown in Eq. (42), the hydrodynamic interaction function satisfies $H(\theta,\theta) = 1$. Owing to Eqs. (50) and (51), the hydrodynamic interaction function also possesses the following symmetry:

$$H(\theta_j+\pi,\theta_k) = -H(\theta_j,\theta_k), \quad (53)$$

$$H(\theta_j,\theta_k+\pi) = -H(\theta_j,\theta_k). \quad (54)$$

Figure 5(a) shows the phase coupling function $\Gamma(\psi)$ given by Eq. (47). As shown in Eq. (48), the phase coupling function satisfies $\Gamma(0) = 1$. Owing to Eq. (51), the phase coupling function also possesses the following symmetry:

$$\Gamma(\psi+\pi) = -\Gamma(\psi). \quad (55)$$

Figure 5(b) shows the antisymmetric component of the phase coupling function, $\Gamma_a(\psi)$, given by Eq. (46). It is observed that the in-phase synchronized solution ($\psi = 0$) is globally stable.

C. Direct numerical simulations

Figure 6 shows the comparison of the effective phase sensitivity function $\zeta(\theta)$ between the direct numerical simulations of Eq. (32) and the theoretical curve shown in Fig. 3(b). In the simulations, we measured the phase response of the beating flagellum at the phase θ by applying a weak impulse uniformly to all the points; subsequently, normalizing the phase response curve by the weak impulse intensity ϵ, we obtained the effective phase sensitivity function $\zeta(\theta)$. The simulation parameters representing the impulse intensity are $\epsilon = 0.01, 0.02$. The simulation results are quantitatively consistent with the theory.

Figure 7 shows the comparison of the time evolution of the phase difference, $\psi(t)/\pi$ vs $\epsilon\omega t$, between the direct numerical simulations of Eq. (38) and the theoretical curve obtained from Fig. 5(b). The simulation parameters representing the effective coupling intensity of hydrodynamic interactions are $\epsilon = 0.001, 0.002$. The simulation results are quantitatively consistent with the theory [40]. It was also confirmed that the in-phase synchronized solution ($\psi = 0$) is globally stable.

IV. CONCLUDING REMARKS

In this paper, we formulated a theory for the phase reduction of a beating flagellum, derived the phase sensitivity function of a beating flagellum, and analyzed the phase synchronization between a pair of beating flagella. The phase reduction theory enabled us to prove the global stability of the in-phase synchronized solution.

Herein, we provide some concluding remarks. First, as observed from Fig. 2(c), the absolute values of the phase sensitivity in the left region are larger than those in the right region. Intuitively, this is because waves propagate from left to right owing to the linear advection term given in Eq. (2). In other words, the upstream region of waves has large absolute values of the phase sensitivity. This property is similar to the results of target waves [34,41,42], in which the pacemaker region as a wave source has large absolute values of phase sensitivity.

Second, as observed from Fig. 5(b), the antisymmetric component of the phase coupling function, $\Gamma_a(\psi)$, is remarkably close to a sinusoidal function [43]. It will be important to quantitatively compare antisymmetric components of phase coupling functions, $\Gamma_a(\psi)$, between theoretical results [e.g., see Fig. 5(b)] and experimental ones (e.g., see Ref. [27]) under the condition in which the two parameters (i.e., c and L) are optimally chosen such that theoretical waveforms of beating flagella most closely resemble experimental ones. It will also be interesting to compare effective phase sensitivity functions $\zeta(\theta)$ between theory [e.g., see Fig. 3(b)] and experiments.

Third, other than the model proposed by Goldstein *et al.* in Ref. [28], there exist some flexible models for a beating flagellum described by partial differential equations [44–50]. A similar theory for phase reduction of such a model can also be formulated. It will be interesting to compare both phase sensitivity functions and phase coupling functions between different flexible models. Moreover, there also exist some models based on a rigid body such as a rigid sphere [51–53] and a rigid cylinder [54,55]. It will also be interesting to examine the difference between the phase coupling functions of a flexible model and a rigid model.

Fourth, as mentioned by Goldstein *et al.* in Ref. [28], Eq. (38), which represents a pair of hydrodynamically coupled beating flagella, can be generalized to an equation that represents a group of hydrodynamically coupled beating flagella exhibiting metachronal waves [56–58]. The phase reduction theory formulated in this paper will also be useful to analyze the equation as well as Eq. (38).

Finally, sponges (Porifera) are known to create water flows by means of beating flagella of choanocytes (collar cells) [59–63]. It is an interesting and challenging problem to reveal whether flagella of choanocytes are synchronized through hydrodynamic interactions and, if so, whether the efficiency of a sponge pump is related to the degree of synchronization. The theory developed in this paper will help us to derive a phase equation that represents beating flagella within a choanocyte chamber, and the derived phase equation will play a vital role in solving the problem.

ACKNOWLEDGMENTS

The authors are grateful to members of MAT/JAMSTEC for helpful comments. Y.K. acknowledges financial support from JSPS (Japan) KAKENHI Grants No. JP17H03279 and No. JP16K17769. R.T. acknowledges financial support from JSPS (Japan) KAKENHI Grants No. JP15K18620 and No. JP15H01604.

APPENDIX A: NUMERICAL METHODS FOR MODEL EQUATIONS

In this Appendix, we describe the numerical scheme for the model equation represented by

$$\frac{\partial}{\partial t}h(x,t) = -c\frac{\partial h}{\partial x} - 2\frac{\partial^2 h}{\partial x^2} - \frac{\partial^4 h}{\partial x^4} + \left(\frac{\partial^2 h}{\partial x^2}\right)^3, \tag{A1}$$

where the boundary condition at the left end ($x = 0$) is given by

$$h(x,t)\Big|_{x=0} = \frac{\partial^2 h(x,t)}{\partial x^2}\Big|_{x=0} = 0 \tag{A2}$$

and the boundary condition at the right end ($x = L$) is given by

$$\frac{\partial^2 h(x,t)}{\partial x^2}\Big|_{x=L} = \frac{\partial^3 h(x,t)}{\partial x^3}\Big|_{x=L} = 0. \tag{A3}$$

Further, the position x is discretized as $x_i = ia$ for $i = 0,1,\ldots,N$ with $a = L/N$, and the variable h at the point x_i is denoted by h_i. As in Refs. [28,64], we apply a second-order finite-difference scheme based on symmetric stencils for the partial differential equation and one-sided stencils for the boundary conditions as follows. First, the central finite-difference scheme of Eq. (A1) is given by the following equation for $i = 2,3,\ldots,N-2$:

$$\begin{aligned}\frac{dh_i}{dt} =& -c\frac{h_{i+1} - h_{i-1}}{2a} - 2\frac{h_{i+1} - 2h_i + h_{i-1}}{a^2} \\ & - \frac{h_{i+2} - 4h_{i+1} + 6h_i - 4h_{i-1} + h_{i-2}}{a^4} \\ & + \left(\frac{h_{i+1} - 2h_i + h_{i-1}}{a^2}\right)^3.\end{aligned} \tag{A4}$$

Second, the forward finite-difference scheme of Eq. (A2) is given by

$$h_0 = 0, \tag{A5}$$

$$h_1 = \frac{4h_2 - h_3}{5}. \tag{A6}$$

Finally, the backward finite-difference scheme of Eq. (A3) is given by

$$h_N = \frac{48h_{N-2} - 52h_{N-3} + 15h_{N-4}}{11}, \tag{A7}$$

$$h_{N-1} = \frac{28h_{N-2} - 23h_{N-3} + 6h_{N-4}}{11}. \tag{A8}$$

APPENDIX B: NUMERICAL METHODS FOR ADJOINT EQUATIONS

In this Appendix, we describe the numerical scheme for the adjoint equation represented by

$$\frac{\partial}{\partial s}z(x,-\omega s) = c\frac{\partial z}{\partial x} - 2\frac{\partial^2 z}{\partial x^2} - \frac{\partial^4 z}{\partial x^4} + 3\frac{\partial^2 (zg)}{\partial x^2},$$
$$g(x,-\omega s) = \left[\frac{\partial^2 h_0(x,-\omega s)}{\partial x^2}\right]^2, \tag{B1}$$

where the adjoint boundary condition at the left end ($x = 0$) is given by

$$z(x,-\omega s)\Big|_{x=0} = \frac{\partial^2 z(x,-\omega s)}{\partial x^2}\Big|_{x=0} = 0 \tag{B2}$$

and the adjoint boundary condition at the right end ($x = L$) is given by

$$\left(2 + \frac{\partial^2}{\partial x^2}\right)z(x,-\omega s)\Big|_{x=L}$$
$$= \left(-c + 2\frac{\partial}{\partial x} + \frac{\partial^3}{\partial x^3}\right)z(x,-\omega s)\Big|_{x=L} = 0. \tag{B3}$$

Further, the position x is discretized as $x_i = ia$ for $i = 0,1,\ldots,N$ with $a = L/N$, and the variable z at the point x_i is denoted by z_i. As in Appendix A, we apply a second-order finite-difference scheme based on symmetric stencils for the adjoint equation and one-sided stencils for the adjoint boundary conditions as follows. First, the central finite-difference scheme of Eq. (B1) is given by the following equation for $i = 2,3,\ldots,N-2$:

$$\frac{dz_i}{ds} = +c\frac{z_{i+1} - z_{i-1}}{2a} - 2\frac{z_{i+1} - 2z_i + z_{i-1}}{a^2}$$
$$- \frac{z_{i+2} - 4z_{i+1} + 6z_i - 4z_{i-1} + z_{i-2}}{a^4}$$
$$+ 3\frac{z_{i+1}g_{i+1} - 2z_i g_i + z_{i-1}g_{i-1}}{a^2}. \tag{B4}$$

Second, the forward finite-difference scheme of Eq. (B2) is given by

$$z_0 = 0, \tag{B5}$$

$$z_1 = \frac{4z_2 - z_3}{5}. \tag{B6}$$

Finally, the backward finite-difference scheme of Eq. (B3) is given by

$$z_N = \frac{(48 - 22a^2)z_{N-2} - (52 - 8a^2)z_{N-3} + 15z_{N-4}}{11 + 22a^2 + 10ca^3 + 16a^4}, \tag{B7}$$

$$z_{N-1} = \frac{(28 + 28a^2 + 8ca^3 + 4a^4)z_{N-2} - (23 + 22a^2 + 2ca^3)z_{N-3} + (6 + 6a^2)z_{N-4}}{11 + 22a^2 + 10ca^3 + 16a^4}. \tag{B8}$$

Moreover, from Eq. (29), the normalization condition for z is given by

$$\frac{a}{2}z_0 u_0 + \sum_{i=1}^{N-1} a z_i u_i + \frac{a}{2}z_N u_N = 1, \tag{B9}$$

where u_i is the value of the Floquet zero eigenfunction U_0 at the point x_i.

[1] A. T. Winfree, *The Geometry of Biological Time* (Springer, New York, 1980); *ibid.*, 2nd ed. (Springer, New York, 2001).

[2] Y. Kuramoto, *Chemical Oscillations, Waves, and Turbulence* (Springer, New York, 1984).

[3] A. Pikovsky, M. Rosenblum, and J. Kurths, *Synchronization: A Universal Concept in Nonlinear Sciences* (Cambridge University Press, Cambridge, 2001).

[4] F. C. Hoppensteadt and E. M. Izhikevich, *Weakly Connected Neural Networks* (Springer, New York, 1997).

[5] E. M. Izhikevich, *Dynamical Systems in Neuroscience: The Geometry of Excitability and Bursting* (MIT Press, Cambridge, MA, 2007).

[6] G. B. Ermentrout and D. H. Terman, *Mathematical Foundations of Neuroscience* (Springer, New York, 2010).

[7] B. Ermentrout, Type I membranes, phase resetting curves, and synchrony, Neural Comput. **8**, 979 (1996).

[8] E. Brown, J. Moehlis, and P. Holmes, On the phase reduction and response dynamics of neural oscillator populations, Neural Comput. **16**, 673 (2004).

[9] H. Nakao, Phase reduction approach to synchronization of nonlinear oscillators, Contemp. Phys. **57**, 188 (2016).

[10] P. Ashwin, S. Coombes, and R. Nicks, Mathematical frameworks for oscillatory network dynamics in neuroscience, J. Math. Neurosci. **6**, 1 (2016).

[11] S. H. Strogatz, From Kuramoto to Crawford: Exploring the onset of synchronization in populations of coupled oscillators, Physica D **143**, 1 (2000).

[12] J. A. Acebrón, L. L. Bonilla, C. J. P. Vicente, F. Ritort, and R. Spigler, The Kuramoto model: A simple paradigm for synchronization phenomena, Rev. Mod. Phys. **77**, 137 (2005).

[13] A. Arenas, A. Díaz-Guilera, J. Kurths, Y. Moreno, and C. Zhou, Synchronization in complex networks, Phys. Rep. **469**, 93 (2008).

[14] A. Pikovsky and M. Rosenblum, Dynamics of globally coupled oscillators: Progress and perspectives, Chaos **25**, 097616 (2015).

[15] F. A. Rodrigues, T. K. D. M. Peron, P. Ji, and J. Kurths, The Kuramoto model in complex networks, Phys. Rep. **610**, 1 (2016).

[16] T. Ishikawa, Suspension biomechanics of swimming microbes, J. R. Soc. Interface **6**, 815 (2009).

[17] E. Lauga and T. R. Powers, The hydrodynamics of swimming microorganisms, Rep. Prog. Phys. **72**, 096601 (2009).

[18] R. Golestanian, J. M. Yeomans, and N. Uchida, Hydrodynamic synchronization at low Reynolds number, Soft Matter **7**, 3074 (2011).

[19] J. Elgeti, R. G. Winkler, and G. Gompper, Physics of microswimmers: Single particle motion and collective behavior: A review, Rep. Prog. Phys. **78**, 056601 (2015).

[20] R. E. Goldstein, Green algae as model organisms for biological fluid dynamics, Annu. Rev. Fluid Mech. **47**, 343 (2015).

[21] E. Lauga, Bacterial hydrodynamics, Annu. Rev. Fluid Mech. **48**, 105 (2016).

[22] R. E. Goldstein, M. Polin, and I. Tuval, Noise and Synchronization in Pairs of Beating Eukaryotic Flagella, Phys. Rev. Lett. **103**, 168103 (2009).

[23] R. E. Goldstein, M. Polin, and I. Tuval, Emergence of Synchronized Beating During the Regrowth of Eukaryotic Flagella, Phys. Rev. Lett. **107**, 148103 (2011).

[24] K. C. Leptos, K. Y. Wan, M. Polin, I. Tuval, A. I. Pesci, and R. E. Goldstein, Antiphase Synchronization in a Flagellar-Dominance Mutant of Chlamydomonas, Phys. Rev. Lett. **111**, 158101 (2013).

[25] K. Y. Wan and R. E. Goldstein, Rhythmicity, Recurrence, and Recovery of Flagellar Beating, Phys. Rev. Lett. **113**, 238103 (2014).

[26] K. Y. Wan, K. C. Leptos, and R. E. Goldstein, Lag, lock, sync, slip: The many 'phases' of coupled flagella, J. R. Soc. Interface **11**, 20131160 (2014).

[27] D. R. Brumley, K. Y. Wan, M. Polin, and R. E. Goldstein, Flagellar synchronization through direct hydrodynamic interactions, eLife **3**, e02750 (2014).

[28] R. E. Goldstein, E. Lauga, A. I. Pesci, and M. R. E. Proctor, Elastohydrodynamic synchronization of adjacent beating flagella, Phys. Rev. Fluids **1**, 073201 (2016).

[29] Y. Kawamura, H. Nakao, and Y. Kuramoto, Collective phase description of globally coupled excitable elements, Phys. Rev. E **84**, 046211 (2011).

[30] Y. Kawamura, Collective phase reduction of globally coupled noisy dynamical elements, Phys. Rev. E **95**, 032225 (2017).

[31] Y. Kawamura and H. Nakao, Collective phase description of oscillatory convection, Chaos **23**, 043129 (2013).

[32] Y. Kawamura and H. Nakao, Noise-induced synchronization of oscillatory convection and its optimization, Phys. Rev. E **89**, 012912 (2014).

[33] Y. Kawamura and H. Nakao, Phase description of oscillatory convection with a spatially translational mode, Physica D **295-296**, 11 (2015).

[34] H. Nakao, T. Yanagita, and Y. Kawamura, Phase-Reduction Approach to Synchronization of Spatiotemporal Rhythms in Reaction-Diffusion Systems, Phys. Rev. X **4**, 021032 (2014).

[35] Y. Kawamura, S. Shirasaka, T. Yanagita, and H. Nakao, Optimizing mutual synchronization of rhythmic spatiotemporal patterns in reaction-diffusion systems, Phys. Rev. E **96**, 012224 (2017).

[36] The physical interpretation of this phenomenological model is as follows: the first term is introduced for breaking the left-right symmetry; the second and fourth terms originate from curvature effects; the third term represents the elasticity. In particular, the second and fourth terms can be considered as a Taylor expansion of a nonlinear function of the curvature up to the cubic term; here, a quadratic term, i.e., $(\partial_x^2 h)^2$, is absent for preserving the up-down symmetry. See Ref. [28] for more details.

[37] D. Zwillinger, *Handbook of Differential Equations*, 3rd ed. (Academic Press, New York, 1998).

[38] J. P. Keener, *Principles of Applied Mathematics: Transformation and Approximation*, 2nd ed. (Perseus, Cambridge, MA, 2000).

[39] We consider a pair of hydrodynamically coupled beating flagella at a low Reynolds number. Here, the radius and length of each flagellum are denoted by r and ℓ, respectively. Further, the mean distance between the two flagella is denoted by d. Under the condition of $r \ll d \ll \ell$, the effective coupling intensity of hydrodynamic interactions is given by the following equation: $\epsilon = \ln(\ell/d)/\ln(\ell/r)$. For example, the effective coupling intensity ϵ becomes small as the mean distance d becomes large. See Ref. [28] for more details.

[40] According to Ref. [28], the effective coupling intensity of hydrodynamic interactions is typically estimated as $\epsilon = 0.25$–0.5. In such a realistic value, a simulation result is not quantitatively consistent with the theory, but they are still qualitatively consistent with each other. Note also that Eq. (38) itself is approximately obtained in the weak coupling regime [28]. In this paper, to further analyze Eq. (38), phase equations are approximately derived by making full use of the weak coupling. In the weak coupling regime, simulation results are quantitatively consistent with the theory.

[41] N. Masuda, Y. Kawamura, and H. Kori, Collective fluctuations in networks of noisy components, New J. Phys. **12**, 093007 (2010).

[42] Y. Kawamura and H. Nakao, Optimization of noise-induced synchronization of oscillator networks, Phys. Rev. E **94**, 032201 (2016).

[43] This is because the limit-cycle solution $h_0(x,\theta)$ shown in Fig. 2(a) is close to sinusoidal as a function of phase θ and, therefore, the Floquet zero eigenfunction $U_0(x,\theta) = \partial h_0(x,\theta)/\partial\theta$ shown in Fig. 2(b) is also close to sinusoidal. Although the phase sensitivity function $Z(x,\theta) = U_0^*(x,\theta)$ shown in Fig. 2(c) contains higher Fourier components of the phase θ, the phase coupling function $\Gamma(\psi)$ given by Eq. (47) is a convolution of $U_0^*(x,\theta)$ and $U_0(x,\theta)$ and, therefore, the phase coupling function $\Gamma(\psi)$ and its antisymmetric component $\Gamma_a(\psi)$ become close to sinusoidal (see Fig. 5).

[44] S. Camalet and F. Jülicher, Generic aspects of axonemal beating, New J. Phys. **2**, 24 (2000).

[45] I. H. Riedel-Kruse, A. Hilfinger, J. Howard, and F. Jülicher, How molecular motors shape the flagellar beat, HFSP J. **1**, 192 (2007).

[46] A. Hilfinger and F. Jülicher, The chirality of ciliary beats, Phys. Biol. **5**, 016003 (2008).
[47] A. Hilfinger, A. K. Chattopadhyay, and F. Jülicher, Nonlinear dynamics of cilia and flagella, Phys. Rev. E **79**, 051918 (2009).
[48] P. V. Bayly and K. S. Wilson, Equations of interdoublet separation during flagella motion reveal mechanisms of wave propagation and instability, Biophys. J. **107**, 1756 (2014).
[49] P. V. Bayly and K. S. Wilson, Analysis of unstable modes distinguishes mathematical models of flagellar motion, J. R. Soc. Interface **12**, 20150124 (2015).
[50] P. Sartori, V. F. Geyer, A. Scholich, F. Jülicher, and J. Howard, Dynamic curvature regulation accounts for the symmetric and asymmetric beats of *Chlamydomonas* flagella, eLife **5**, e13258 (2016).
[51] N. Uchida and R. Golestanian, Synchronization and Collective Dynamics in a Carpet of Microfluidic Rotors, Phys. Rev. Lett. **104**, 178103 (2010).
[52] N. Uchida and R. Golestanian, Generic Conditions for Hydrodynamic Synchronization, Phys. Rev. Lett. **106**, 058104 (2011).
[53] Y. Izumida, H. Kori, and U. Seifert, Energetics of synchronization in coupled oscillators rotating on circular trajectories, Phys. Rev. E **94**, 052221 (2016).
[54] A. Takamatsu, T. Ishikawa, K. Shinohara, and H. Hamada, Asymmetric rotational stroke in mouse node cilia during left-right determination, Phys. Rev. E **87**, 050701(R) (2013).
[55] A. Takamatsu, K. Shinohara, T. Ishikawa, and H. Hamada, Hydrodynamic Phase Locking in Mouse Node Cilia, Phys. Rev. Lett. **110**, 248107 (2013).
[56] D. R. Brumley, M. Polin, T. J. Pedley, and R. E. Goldstein, Hydrodynamic Synchronization and Metachronal Waves on the Surface of the Colonial Alga Volvox Carteri, Phys. Rev. Lett. **109**, 268102 (2012).
[57] D. R. Brumley, M. Polin, T. J. Pedley, and R. E. Goldstein, Metachronal waves in the flagellar beating of *Volvox* and their hydrodynamic origin, J. R. Soc. Interface **12**, 20141358 (2015).
[58] J. Elgeti and G. Gompper, Emergence of metachronal waves in cilia arrays, Proc. Natl. Acad. Sci. USA **110**, 4470 (2013).
[59] P. S. Larsen and H. U. Riisgård, The sponge pump, J. Theor. Biol. **168**, 53 (1994).
[60] H. U. Riisgård and P. S. Larsen, Particle capture mechanisms in suspension-feeding invertebrates, Mar. Ecol. Prog. Ser. **418**, 255 (2010).
[61] S. P. Leys, G. Yahel, M. A. Reidenbach, V. Tunnicliffe, U. Shavit, and H. M. Reiswig, The sponge pump: The role of current induced flow in the design of the sponge body plan, PLoS ONE **6**, e27787 (2011).
[62] J. L. Mah, K. K. Christensen-Dalsgaard, and S. P. Leys, Choanoflagellate and choanocyte collar-flagellar systems and the assumption of homology, Evol. Dev. **16**, 25 (2014).
[63] R. Tsubaki and M. Kato, A novel filtering mutualism between a sponge host and its endosymbiotic bivalves, PLoS ONE **9**, e108885 (2014).
[64] A.-K. Tornberg and M. J. Shelley, Simulating the dynamics and interactions of flexible fibers in Stokes flows, J. Comput. Phys. **196**, 8 (2004).